Hyperbolic orbits in the Solar system: interstellar origin or perturbed Oort cloud comets?

Arika Higuchi [1]★ and Eiichiro Kokubo[2]

[1]*RISE Project, National Astronomical Observatory of Japan, Osawa, Mitaka, Tokyo 181-8588, Japan*
[2]*Division of Science, National Astronomical Observatory of Japan, Osawa, Mitaka, Tokyo 181-8588, Japan*

ABSTRACT

We study the dynamical properties of objects in hyperbolic orbits passing through the inner Solar system in the context of two different potential sources: interstellar space and the Oort cloud. We analytically derive the probability distributions of eccentricity, e, and perihelion distance, q, for each source and estimate the numbers of objects produced per unit of time as a function of these quantities. By comparing the numbers from the two sources, we assess which origin is more likely for a hyperbolic object having a given eccentricity and perihelion distance. We find that the likelihood that a given hyperbolic object is of interstellar origin increases with decreasing eccentricity and perihelion. Conversely, the likelihood that a hyperbolic object has been scattered from the Oort cloud by a passing star increases with decreasing eccentricity and increasing perihelion. By carefully considering their orbital elements, we conclude that both 1I/2017 U1 'Oumuamua ($e \simeq 1.2$ and $q \simeq 0.26$ au) and 2I/2019 Q4 Borisov ($e \simeq 3.3$ and $q \simeq 2$ au) are most likely of interstellar origin, not scattered from the Oort cloud. However, we also find that Oort cloud objects can be scattered into hyperbolic orbits like those of the two known examples, by sub-stellar and even sub-Jovian mass perturbers. This highlights the need for better characterization of the low-mass end of the free-floating brown dwarf and planet population.

**Key words:** comets: general – Oort cloud.

1 INTRODUCTION

The standard formation scenario of planetary systems naturally suggests that interstellar space is filled with many planetesimals because exo-giant planets eject planetesimals during planet formation, as the planets in the Solar system did (e.g. Dones et al. 2004). Planetesimals that are almost but not completely ejected from the planetary system survive as Oort cloud comets in the planetary system. Oort cloud comets become observable from Earth when their perihelion distances become small due to external forces. For example, when a star penetrates the Oort cloud, the star drills a narrow tunnel through the Oort cloud by ejecting the comets within some distance from the star as described in Fig. 1. Some of the ejected comets make a last perihelion passage as their farewell to the Solar system before becoming fully interstellar objects. In other words, both interstellar space and the Oort cloud are possible as sources of objects moving along hyperbolic orbits.

1I/2017 U1 'Oumuamua, (hereafter U1) is the first highly eccentric ($e \simeq 1.2$) object identified in the Solar system, with

an effective velocity at infinity $V \simeq 26$ km s^{-1} (e.g. Williams 2017). This velocity cannot be explained by planetary perturbations because U1 did not encounter any of the planets (Meech et al. 2017). Many observations of U1's shape, thermal properties, colours, absence of cometary activity, tumbling rotational state, and non-gravitational acceleration have been reported (e.g. Bannister et al. 2017; Jewitt et al. 2017; Knight et al. 2017; Meech et al. 2017; Ye et al. 2017; Bolin et al. 2018; Fraser et al. 2018; Micheli et al. 2018) and are summarized in 'Oumuamua ISSI Team (2019). Peculiar physical properties of U1 include its extremely elongated or oblate (Mashchenko 2019) shape and its lack of cometary activity. Together, these properties are unlike those found in other small Solar system objects. However, physical peculiarities alone are not enough to exclude the possibility that U1 might be a Solar system body deflected from the Oort cloud. We examine this possibility here. A second hyperbolic object, the comet C/2019 Q4 (2I/Borisov, hereafter Q4), was discovered by G. Borisov on 2019 August 30, observing from MARGO, Nauchnij, in the Crimean peninsula.[1]

★ E-mail: higuchi.arika@nao.ac.jp

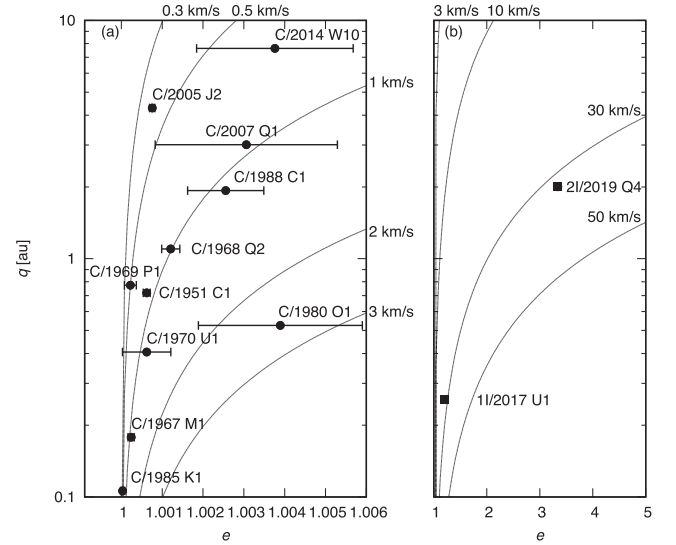[1]MPEC 2019-R106: COMET C/2019 Q4 (Borisov) https://minorplanetcenter.net/mpec/K19/K19RA6.html.
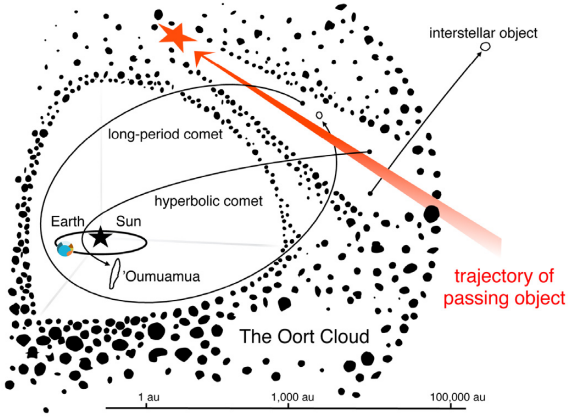
Figure 1. Schematic illustration of the penetration of a star through the Oort cloud. The star scatters comets away along the trajectory and generates long-period comets, hyperbolic comets, and interstellar objects.

Figure 2. Original eccentricities and perihelion distances of originally in hyperbolic orbits. (a) 11 comets listed in table 1 in Królikowska & Dybczyński (2019). (b) 1I/2017 U1 ('Oumuamua) and 2I/2019 Q4 (Borisov). Equi-V curves from equation (14) for $V = 0.3$, 0.5, 1, 2, 3, 10, 30, and 50 km s^{-1} are shown with thin dashed curves.

Soon after that the Q4's interstellar nature was confirmed.[2] Q4 has a very high eccentricity of $e = 3.3$, a comet-like appearance and spectrum similar to those of D-type asteroids (de León et al. 2019; Fitzsimmons et al. 2019; Jewitt & Luu 2019).

While most long-period comets have $e < 1$, some are known with $e \gtrsim 1$. Królikowska & Dybczyński (2017) calculated the orbits of long-period comets carefully taking into account the perturbations from planets and the non-gravitational forces to infer their original elements, defined as the orbital elements at 250 au from the Sun before the perihelion passage (e.g. Królikowska 2014; Królikowska & Dybczyński 2017). Królikowska & Dybczyński (2019) collected data for a full sample of long-period comets discovered over the 1801–2017 period and calculated their original orbital elements. They used the JPL Small Body Database Search Engine[3] to construct a complete list of long-period comets discovered since 1801, omitting sungrazing comets. They found that, in most cases, the comets followed elliptical (bound) orbits prior to their last perihelion. Fig. 2(a) shows the original eccentricities e_{orig} and perihelion distances q_{orig} of 11 comets in original, marginally hyperbolic orbits from table 1 in Królikowska & Dybczyński (2019). While these comets could also come from the interstellar space, it is more likely that their eccentricities exceed unity only because of uncertainties in the astrometry. In that case, comets in Fig. 2(a) are dynamically the same as other long-period comets, but different from U1 and Q4 shown in Fig. 2(b).

Here, we derive analytically the probability distributions of eccentricity, e, and perihelion distance, q, for hyperbolic orbits derived from either interstellar space or the Oort cloud. We estimate the ratio of numbers of objects from the two sources and the dependence of this ratio on various parameters of the Oort cloud and the interstellar objects.

In Section 2, we describe the derivation of the likelihood that interstellar objects have a given value of b, the impact parameter to the Sun and V, the velocity at infinity. Section 3 follows the methodology applied in Section 2 but for the production of comets scattered from the Oort cloud on hyperbolic orbits. In Section 4, we plot the probabilities derived in Sections 2 and 3 on the e versus q plane and make comparison between interstellar objects

and hyperbolic Oort cloud comets. In Section 5, we compare the expected numbers of interstellar objects and hyperbolic Oort cloud comets with an assumption that the Solar system recently had an encounter with a passing object. The properties of a passing object implied by the orbits of U1 and Q4 are discussed in Section 6. Section 7 gives a summary and discussion.

2 INTERSTELLAR OBJECTS

Assuming a uniform spatial distribution and a Maxwellian velocity distribution, the number of interstellar objects (hereafter ISOs) encountering the Sun with the velocity at infinity between V and $V + \delta V$ and the impact parameter between b and $b + \delta b$ per time is given by

$$\delta N_{\mathrm{ISO}}(V, b) = 2\pi b \delta b \delta V \rho_{\mathrm{ISO}} p(V) \delta V, \tag{1}$$

where ρ_{ISO} is the total number density of ISOs and $p(V)$ is a Maxwellian distribution,

$$p(V) = \sqrt{\frac{2}{\pi}} V^2 \exp\left(-\frac{V^2}{2a^2}\right) a^{-3}, \tag{2}$$

where $a = \sqrt{\pi/8} \langle V \rangle$ and $\langle V \rangle$ is the mean velocity. We assume that ISOs are planetesimals ejected from planetary systems by scattering from giant planet(s). Other fragments might be generated by tidal disruption of planets (Ćuk 2018; Rafikov 2018) but their expected contribution is small and neglected here. We estimate the number density of ISOs generated by stars of spectral type 'i' as

$$\rho_{\mathrm{ISO}}^i = \rho_{\mathrm{star}}^i p_{\mathrm{gp}}^i n_{\mathrm{OC}}^i k_{\mathrm{ISO}}, \tag{3}$$

where ρ_{star}^i is the number density of the stars, p_{gp}^i is the probability that the stars have one of more giant planets, n_{OC}^i is the number of comets in the Oort cloud around each star, and k_{ISO} is set so that $n_{\mathrm{OC}}^i k_{\mathrm{ISO}}$ gives the number of ISOs generated by a star of type 'i'. We use ρ_{star} in García-Sánchez et al. (2001) and for simplicity set $p_{\mathrm{gp}}^i =0.015$, 0.1, and 0 for MK, GFA, and other type stars, respectively (Moro-Martín, Turner & Loeb 2009). Assuming that

Table 1. Stellar parameters used in this paper. 'wd' and 'gi' indicate white dwarfs and giant stars, respectively. The last column gives the mean heliocentric velocity. The values are taken from García-Sánchez et al. (2001), Moro-Martín et al. (2009), and Rickman et al. (2008).

Type	m_*^i ($m_\odot$)	$\rho_{\rm star}^i$ (10^{-3} pc^{-3})	$p_{\rm gp}^i$	V_* (km s^{-1})
B0	9	0.06	0	24.6
A0	3.2	0.27	0	27.5
A5	2.1	0.44	0.1	29.3
F0	1.7	1.42	0.1	36.5
F5	1.3	0.64	0.1	43.6
G0	1.1	1.52	0.1	49.8
G5	0.93	2.34	0.1	49.6
K0	0.78	2.68	0.015	42.6
K5	0.69	5.26	0.015	54.3
M0	0.47	8.72	0.015	50.0
M5	0.21	41.55	0.015	51.8
wd	0.9	3.0	0	80.2
gi	4	0.43	0	49.7

the number of Oort cloud comets is proportional to the mass of the parent star m_*^i, we set $n_{\rm OC}^i = n_{\rm OC}^{\rm SS}(m_*^i/m_\odot)$, where $n_{\rm OC}^{\rm SS}$ is the number of Oort cloud comets in the Solar system. We use m_*^i summarized by Rickman et al. (2008), substituting all the values assumed above and summing over all the stellar types, to obtain the total number density of ISOs as

$$\rho_{\rm ISO} = n_{\rm OC}^{\rm SS} k_{\rm ISO} \sum_{i=0}^{13} \rho_{\rm star}^i p_{\rm gp}^i \left(\frac{m_*^i}{m_\odot} \right) \simeq \Gamma n_{\rm OC}^{\rm SS} k_{\rm ISO} , \tag{4}$$

where $\Gamma \simeq 10^{-3}$ [pc^{-3}]. Table 1 lists our adopted values. We assume that the velocity distribution of ISOs is similar to that of their parent stars, which is $\langle V \rangle \simeq 50$ km s^{-1} as summarized in Table 1 (Rickman et al. 2008). This value is larger than the velocity of the Sun with respect to the Local Standard of Rest ($\lesssim 20$ km s^{-1}), which previous studies used (e.g. Moro-Martín et al. 2009; Engelhardt et al. 2017) Substituting equations (2) and (4) into equation (1), we obtain

$$\delta N_{\rm ISO}(V, b) = C_{\rm ISO} \delta V \delta b, \tag{5}$$

where $C_{\rm ISO}$ is the number density of ISOs with a given V and b, written as

$$C_{\rm ISO} = 2\pi \Gamma n_{\rm OC}^{\rm SS} k_{\rm ISO} \, V \, p(V) \, b. \tag{6}$$

3 HYPERBOLIC OORT CLOUD COMETS

We first derive the velocity and impact parameter of a hyperbolic Oort cloud comet (hereafter HOC) against the Sun after an encounter with a passing object by using the two-body scattering formula. Then, we derive the expected number of HOCs for given V and b by taking into account the number density of comets in the Oort cloud.

3.1 Velocity and impact parameter given by a passing object

We assume that an object that approaches the Sun passes on a straight trajectory. We describe each encounter of the object with a comet using the following parameters: m_* and V_*, the mass and velocity of the object, $b_{\rm Sun}$, the impact parameter of the object to the Sun, $\boldsymbol{b}_{\rm HOC}$, the impact parameter vector from the comet to the object, and $\boldsymbol{r}_*$, the position vector of the object from the Sun at the moment when the object has the closest approach to the comet. We assume that the comet is not moving relative to the Sun and V and b of scattered comets are determined only by the perturber. Also

considering $b_{\rm Sun} \gg b_{\rm HOC}$, we approximate the position vector of the comet from the Sun with $\boldsymbol{r} = \boldsymbol{r}_*$.

The angle between the velocity vectors of the comet to the object before and after the encounter θ is given as a function of only V and V_*. The angle θ determines the position of the object at the encounter so that the comet has an orbit with b after the encounter (Appendix A1). We find r_* that gives V and b as (Appendix A2),

$$r_* = b_{\rm Sun} \left(1 - \frac{V^2}{4V_*^2} \right)^{-\frac{1}{2}}. \tag{7}$$

3.2 Expected number of HOCs per unit of time

We estimate the number of HOCs encountering the Sun with a velocity between V and $V + \delta v$ and an impact parameter between b and $b + \delta b$ per unit of time as

$$\delta N_{\rm HOC} = p_{\rm se} \delta g \rho_{\rm OC}(r), \tag{8}$$

where $p_{\rm se}$ is a probability of having an encounter with an object and δg is an element of volume per unit of time (dimensions of $l^3 \, t^{-1}$) placed at distance $b_{\rm HOC}$ from the passing object,

$$\delta g = \frac{8(Gm_*)^2}{V_* b_{\rm Sun}} V^{-3} \delta V \delta b, \tag{9}$$

and $\rho_{\rm OC}(r)$ is the number density of comets in the Oort cloud at r. The probability $p_{\rm se}$ is 1 if the Solar system just had an encounter with an object, and if not, $p_{\rm se} = 0$. The value of $p_{\rm se}$ averaged over the age of the Solar system is discussed in Section 6. The element of volume per unit time, δg, is defined so that comets contained within δg have a velocity between V and $V + \delta V$ and an impact parameter between b and $b + \delta b$ (Appendix A3). We model the distribution of comets in the Oort cloud as $\rho_{\rm OC}(r) = \bar{\rho}_0 n_{\rm OC}^{\rm SS} r^{-\gamma}$. Numerical studies show $\gamma \sim 3$ (e.g. Dones et al. 2004). Assuming that the Oort cloud has inner and outer edges at $r_{\rm min}$ and $r_{\rm max}$, respectively, we have

$$\bar{\rho}_0 = \begin{cases} \dfrac{(\gamma - 3)}{4\pi} r_{\rm min}^{\gamma-3} & \text{for } \gamma > 3 \\ \left[4\pi \log \left(\dfrac{r_{\rm max}}{r_{\rm min}} \right) \right]^{-1} & \text{for } \gamma = 3 \end{cases}, \tag{10}$$

where we assume $r_{\rm min} \ll r_{\rm max}$ for $\gamma > 3$. Substituting equations (9) and (10) into equation (8), we obtain

$$\delta N_{\rm HOC}(V, b) = C_{\rm HOC} \, \delta V \delta b, \tag{11}$$

where $C_{\rm HOC}$ is the number density of HOCs at a given V and b and using equation (7) written as

$$C_{\rm HOC} = \frac{8(Gm_*)^2}{V_*} \bar{\rho}_0 n_{\rm OC}^{\rm SS} b_{\rm Sun}^{-(\gamma+1)} \left(1 - \frac{V^2}{4V_*^2} \right)^{\frac{1}{2}\gamma} V^{-3}. \tag{12}$$

4 DISTRIBUTIONS OF ECCENTRICITY AND PERIHELION DISTANCE

We convert the distributions of V and b into those of e and q assuming that all objects move on hyperbolic orbits whose focus is at the Sun (Appendix A4). The numbers of ISOs and HOCs encountering the Sun with eccentricity between e and $e + \delta e$ and the perihelion distance between q and $q + \delta q$ per time is given by

$$\delta n(e, q) = C J \delta e \delta q = \delta n(V, b) J, \tag{13}$$
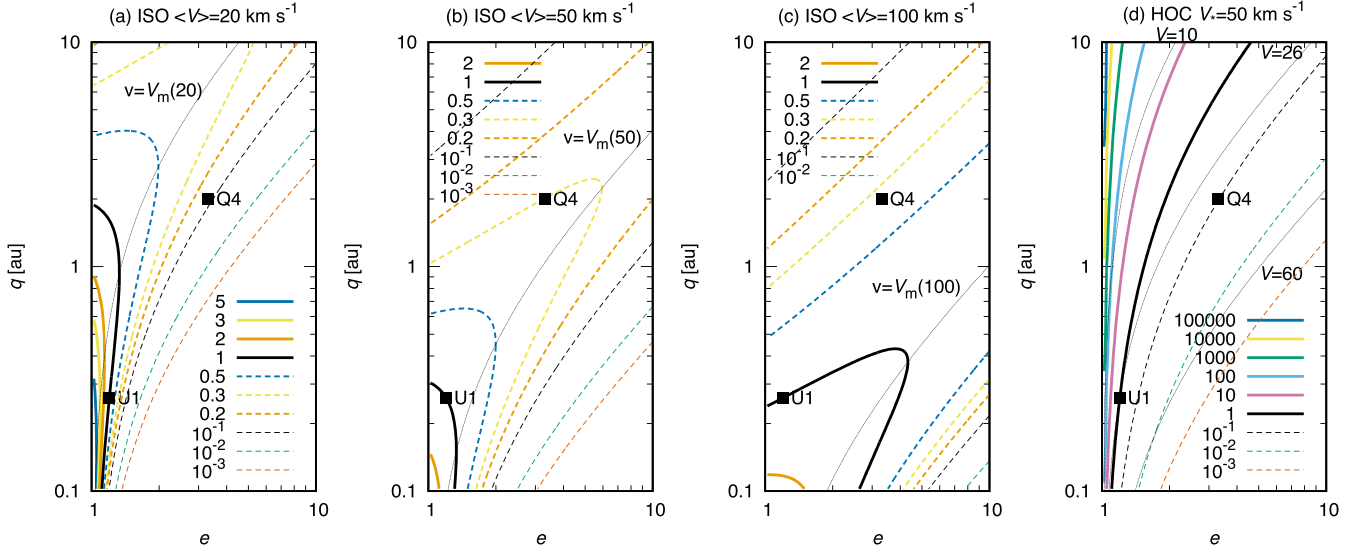
Figure 3. Panels (a), (b), and (c): Scaled contours of the two-dimensional probability distributions plotted on the e versus q plane for ISOs for $\langle V \rangle = 20$ km s^{-1} (a), 50 km s^{-1} (b), and 100 km s^{-1} (c) and an equi-V curve for each $V_m(\langle V \rangle)$ (thin black curve). Panel (d): Scaled contours of the two-dimensional probability distributions integrated over an encounter with an object with $V_* = 50$ km s^{-1} plotted on the e versus q plane and equi-V curves for $V = 10$, 26, and 60 km s^{-1} (thin black curves). Black squares in each panel indicate U1 and Q4.

where $\delta n(V, b)$ and C represent $\delta N_{\mathrm{ISO}}(V, b)$ or $\delta N_{\mathrm{HOC}}(V, b)$ and C_{ISO} or C_{HOC}, respectively, and J is the determinant of the Jacobian between the (V, b) and (e, q) frames.

Panels (a), (b), and (c) in Fig. 3 show the contours of the two-dimensional probability distributions for ISOs obtained from equations (5) and (13) on the e versus q plane. The values of the contours are normalized at U1: we call this normalized probability $p_{\mathrm{ISO}}(e, q)$. We adopt $\langle V \rangle = 20$, 50, and 100 km s^{-1}.

For any value of $\langle V \rangle$ shown in Fig. 3, the probability increases with decreasing e and q. The ridge roughly following the equi-velocity curve given by

$$V = \sqrt{\frac{Gm_\odot(e - 1)}{q}} \tag{14}$$

for each mode $V_m(\langle V \rangle) = (\sqrt{\pi}/2)\langle V \rangle$ is seen, however, the distribution is rather flat. The probability at the same eccentricity as U1's but at $q = 1$ au, is given by $p_{\mathrm{ISO}}(e = 1.2, q = 1) \simeq 1.3$, 0.34, 0.28, for $\langle V \rangle = 20$, 50, and 100 km s^{-1}, respectively. The probability at Q4's e and q is given by $p_{\mathrm{ISO}}(e = 3.3, q = 2) \simeq 0.12$, 0.30, 0.34 for $\langle V \rangle = 20$, 50, and 100 km s^{-1}, respectively. This implies that U1's orbit is more typical of ISOs than Q4's.

For HOCs, we examine the probability distribution of e and q not per unit of time but over an encounter with an object because it varies with time during the encounter. We weight equation (12) by $2b/\sin\alpha$, the path-length of the object where it can generate comets with given V and b (see Fig. 4). Fig. 3(d) shows the probability distribution obtained from equations (11) and (13) on the e versus q plane for HOCs integrated over an encounter with an object with $V_* = 50$ km s^{-1}. The probability diverges at $e = 1$ and $q \to \infty$ ($p_{\mathrm{HOC}} \propto q^{2.5}$). We obtain that $p_{\mathrm{HOC}}(e = 1.2, q = 1)$ is $\simeq 10$. The distribution is steep compared to that of ISOs where e is small. This result barely changes with V_*. The black dotted lines in Fig. 3(d) show the equi-velocity curves for $V = 10$, 26, and 60 km s^{-1}. Comets on equi-velocity curves arrive at the Sun almost at the same time since $b \ll b_{\mathrm{Sun}}$. At $q = 1$ au on the $V = 26$ km s^{-1} − curve, $p(e = 1.76, q = 1) \simeq 0.4$. This implies that, among the HOCs $V = 26$ km s^{-1} that arrive at the Sun around the same time, U1's
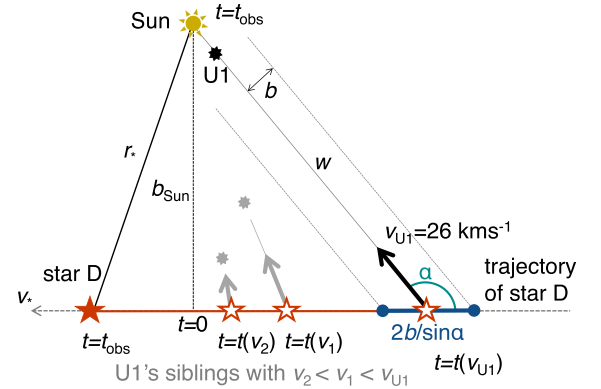

Figure 4. Geometry among the Sun, Star D (a passing object), U1, and U1's siblings plotted on the plane that contains the Sun and the trajectory of Star D, as an example of the HOC production. Star D passes b_{Sun} at $t = 0$. U1 arrives at the Sun at $t = t_{\mathrm{obs}}$.

e and q are as likely for an origin as HOCs as much as ISOs. The arrival time is calculated as $t_{\mathrm{obs}}(V) = w/V - (w/\tan\alpha)/V_* \simeq b_{\mathrm{Sun}}[1 - (3/8)(V/V_*)^2]/V$ for $V/V_* < 1$, where w is the path-length of the HOC (see Fig. 4). This means that the HOCs with larger V arrive at the Sun earlier than those with smaller V. In other words, the advance members of a comet shower are more consistent with U1 than other comets coming after them. Note that $p_{\mathrm{HOC}}(e, q)$ is independent of m_* and b_{Sun}.

5 RATIO OF ISO TO HOC

Integration of equations (5) and (11) over ranges of given eccentricity and perihelion distance gives the absolute numbers of ISOs and HOCs per time. However, we prefer to discuss ratio of ISOs to HOCs, because their absolute numbers strongly depend on the uncertain size distributions. In what follows, we have implicitly assumed that ISOs and HOCs have the same size–frequency distributions, allowing $n_{\mathrm{OC}}^{\mathrm{SS}}$ to be cancelled out.
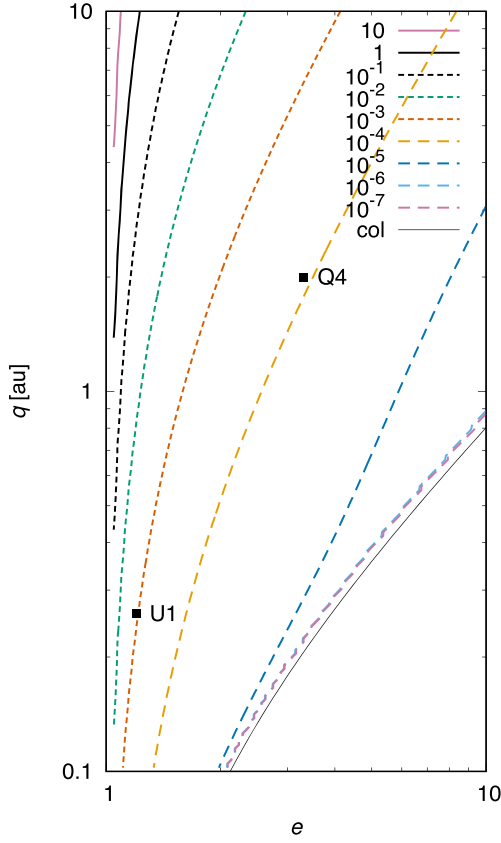
Figure 5. Contours of ratios of the number of HOCs to that of ISOs on the e versus q plane, obtained from equation (15) for $\gamma = 3$, $b_{Sun} = 10^4$ au, m_* $= 10^{-2}\,m_\odot$, $V_* = 50$ km s^{-1}, and $\langle V \rangle = 50$ km s^{-1}. Thin black curve shows equation (16). Black squares indicate U1 and Q4.

We define the ratio of the number of HOCs to that of ISOs for given e and q as

$$\mathcal{H} = \frac{\delta N_{HOC}}{\delta N_{ISO}} = \frac{C_{HOC}}{C_{ISO}}, \qquad (15)$$

which tells us which source is more likely given a particular e and q pair. We assume that an encounter of the Solar system with an object HOC occurs and set $p_{se} = 1$.

Fig. 5 shows contours of $\mathcal{H}$ on the e versus q plane for $\langle V \rangle =$ 50 km s^{-1}, $b_{Sun} = 10^4$ au, $m_*/m_\odot = 10^{-2}$, and $V_* = 50$ km s^{-1}. Other parameters are fixed at $\Gamma = 10^{-3}$, $k_{ISO} = 10$, and $\gamma = 3$. At the e and q of U1 and Q4 in Fig. 5, $\mathcal{H} \sim 10^{-3}$ and $\sim 10^{-4}$, respectively. This means that both U1 and Q4 would be less likely to be HOCs, even if the Solar system had a recent encounter with a passing object as assumed above. One can easily calculate $\mathcal{H}$ for any b_{Sun}, m_*, γ, and k_{ISO} from Fig. 5 as the dependence of $\mathcal{H}$ on b_{Sun} and m_* is simply $\mathcal{H} \propto b_{Sun}^{-(\gamma+1)} m_*^2 \gamma^{-1} k_{ISO}^{-1}$ (equation 12). For $b_{Sun} =$ 10^3 au, $\mathcal{H} \sim 10$ and ~ 1 at the e and q of U1 and Q4, respectively. The overall trend of $\mathcal{H}$ on the e versus q plane does not change with any of the parameters; diverge at $e = 1$ and $q = \infty$. however, note that there are lower limits of m_* for HOC production defined by the condition to avoid a collision between a comet and the passing object (equation 16) and the lower limit of $V_* > V/2$ (equation A3). There is no HOC below the curve showing equation (16) in Fig. 5.

Alternatively to Fig. 5, we can derive the condition for a passing object to generate hyperbolic minor bodies having an origin in the Oort cloud (HOCs) with equal probability to that of being ISOs, by setting $\mathcal{H} = 1$. Fig. 6 shows curves for $\mathcal{H} = 1$ for given e and q on the $b_\odot - V_*$ Pl plane for several m_* and $\langle V \rangle$. Panels (a), (b), and (c)
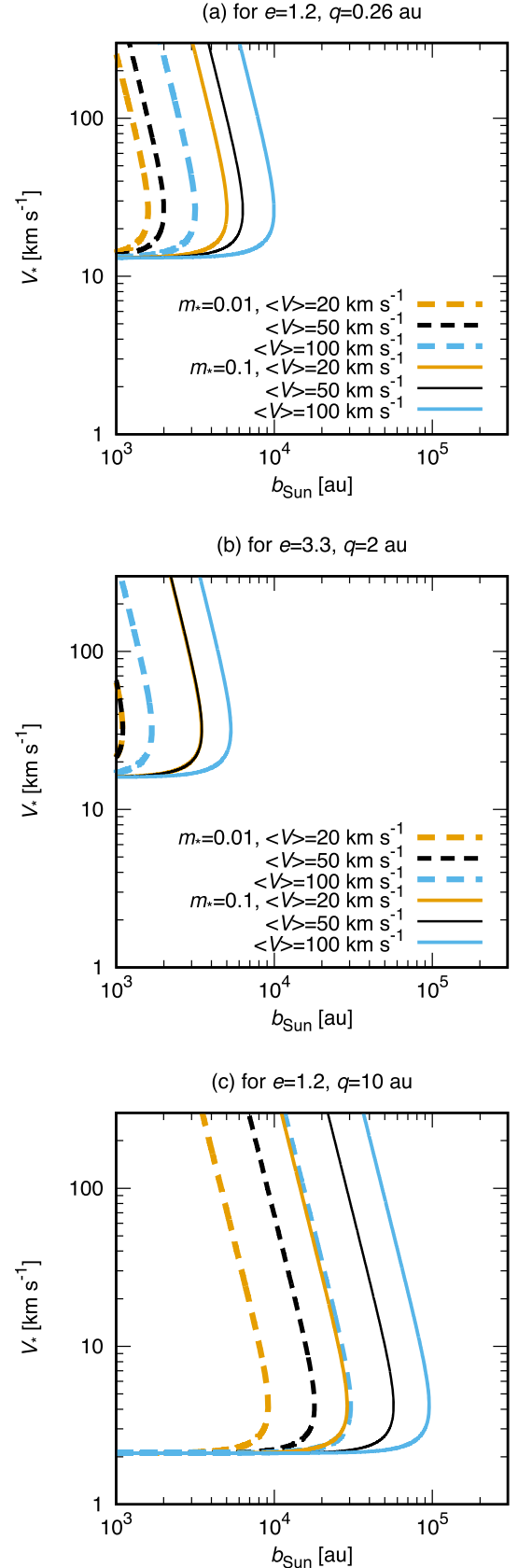
Figure 6. Curves for $H_{HOC/ISO} = 1$ for given e and q on the $b_\odot - V_*$ plane obtained by solving equation (15) = 1 for $\langle V \rangle = 20$ km s^{-1} (orange), 50 km s^{-1} (black), 100 km s^{-1} (blue), and $m_*/m_\odot = 10^{-2}$ (dashed) and 10^{-1} (solid). Panels (a), (b), and (c) are for $(e, q) = (1.2, 0.26)$, $(3.3, 2)$, and $(1.2, 10)$, respectively.

in Fig. 6 are for $(e, q) = (1.2, 0.26)$, $(e, q) = (3.3, 2)$, and $(e, q) = (1.2, 10)$, respectively. Closed areas between the curves and the y-axis in Fig. 6 show the range for passing objects to have $\mathcal{H} = 1$. The curve is roughly defined by a horizontal line at the lower limit of V_* and a diagonal line for constant $b_{Sun}^{(\gamma+1)}V_*$. Figs 6(a) and (b) clearly show that a close encounter with $b_{Sun} \sim 10^3$ au is required for $\mathcal{H} > 1$ if m_* is as small as $\sim 0.01\ m_\odot$. The range for $\mathcal{H} > 1$ becomes larger for larger q. If we can observe objects with q up to 10 au, an encounter with an object with $m_* = 0.01\ m_\odot$ and $b_{Sun} \sim 10^4$ au is enough for $\mathcal{H} > 1$ (Fig. 6c).

6 PROPERTIES OF A HYPOTHETICAL PERTURBER

Suppose a hypothetical object, which we will call 'Star D', scattered an Oort cloud comet on to a hyperbolic object with the velocity at infinity, V. What can we say about the current position and the mass-range of Star D and about the averaged encounter frequency of the Solar system with similar objects?

We assume that Star D is moving along a straight trajectory shown in Fig. 4. The distance travelled since the instant of time that corresponds to the encounter with Star D until now is estimated from $l = b_\odot/\sin\alpha$ and, for Star D, $l_* = lV_*/V$. Then the distance to the Sun from the current position of Star D is approximated by equation (A8). In three-dimensional space, the geometry of the trajectory of Star D and $\boldsymbol{r}_*$ is axisymmetric about the trajectory of U1. Therefore, equation (A8) defines a torus-like volume with a cross-section given by the uncertainties of $b_\odot$ and V_*. Star D has $r_* \simeq 2b_\odot$ for $V_* = 50$ km s^{-1}, where $b_\odot \leq r_{max} \sim 10^5$ au to penetrate the Oort cloud.

A lower limit to the mass of Star D, m_D^{min}, is set by the requirement to avoid a collision, which occurs when impact parameter required to give V (equation A13) becomes smaller than the physical radius of Star D. This leads to

$$m_D^{min} = \left(\frac{3}{4\pi G^3}\right)^{\frac{1}{2}} \rho_*^{-\frac{1}{2}} V_*^3 \left(\frac{4V_*^2}{V^2} - 1\right)^{-\frac{3}{4}}, \quad (16)$$

where V_* and ρ_* are the velocity and density of Star D. Fig. 7 shows the contours of m_D^{min} derived from equations (14) and (16) on the e versus q plane for $V_* = 50$ km s^{-1} and $\rho_* = 10^3$ kg m^{-3}. We have $m_D^{min} \simeq 2 \times 10^{-4}\ m_\odot$ for the production of both U1 ($V \simeq 26$ km s^{-1}) and Q4 ($V \simeq 32$ km s^{-1}). This corresponds to ~ 0.2 Jupiter masses. For the other ($e \sim 1$) comets in Fig. 2(a), we have $m_D^{min} \lesssim 10^{-5}\ m_\odot$ (a few Earth masses).

An upper limit to the mass of Star D, m_D^{max}, can be set by the fact that Star D has not been found by the *Wide-Field Infrared Survey Explorer* (*WISE*; Wright et al. 2010). The free-floating planetary-mass object closest to the Sun is *WISE* j085510.83−071442.5 (Luhman 2014). Its distance and mass are estimated, respectively, as 2.23 ± 0.04 pc (Luhman & Esplin 2016) and 3–10 Jovian masses, assuming an age of 1–10 Gyr (Luhman 2014). Taking this as a measure of the sensitivity of *WISE* to nearby sub-stellar objects, any Jovian mass object with the same brightness as the closest one would have been detected within 1–1.5 pc. The detection capability of *WISE* and the relation between the brightness and the mass of Star D are required to give m_D^{max}. If m_D^{max} is larger than m_D^{min}, there is a possibility that U1 is an Oort cloud comet injected by an object.

The averaged encounter frequency of the Solar system with the candidates for Star D might be estimated from that for stars. Summing up the encounter frequencies of the Solar system with main-sequence stars, white dwarfs, and giant stars given in table 1 in Rickman et al. (2008), we obtain $\simeq 10.5$ stellar encounters per
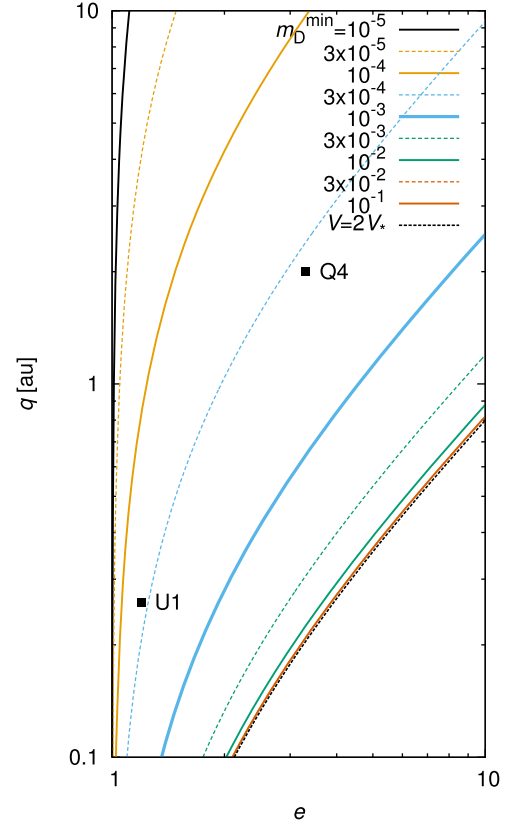
Figure 7. Contours of m_D^{min} derived from equations (14) and (16) on the e versus q plane for $V_* = 50$ km s^{-1} and $\rho_* = 10^3$ kg m^{-3}. Black dotted curve shows $V = 2V_*$ (no solution below this curve). Black squares indicate U1 and Q4.

Myr within 1 pc. This is a lower limit because planetary mass objects have not been taken into account in Rickman et al. (2008) but may nevertheless scatter comets, as estimated in equation (16). The encounter frequency with such small objects over the age of the Solar system cannot yet be reliably estimated. Gravitational microlensing is the only method capable of exploring the entire population of free-floating planets down to mars-mass objects. Although this issue is far from well understood (Sumi et al. 2011; Mróz et al. 2019), some authors (Mróz et al. 2019) have given a value for the upper limit of the frequency of Jupiter-mass free-floating or wide-orbit planets of 0.25 planets per main-sequence star. We give $p_{se} = 1$ in equation (8) to compare the numbers of ISOs and HOCs when we have HOCs (otherwise $\delta N_{HOC} = 0$).

7 SUMMARY AND DISCUSSION

We analytically derive the expected distributions of eccentricity, e, and perihelion distance, q, for objects belonging to two distinct populations. First, we consider initially unbound objects entering the Solar system from interstellar space (ISOs). Secondly, we consider initially bound objects from the Oort cloud (HOCs) scattered on to hyperbolic trajectories by gravitational interaction with a passing star (see Fig. 3). We estimate the numbers of ISOs and HOCs and evaluate them by using their ratio, $\mathcal{H}$, on the e versus q plane (Fig. 5).

(1) We find that hyperbolic objects with small e and small q are the most likely to have an interstellar origin. Conversely, hyperbolic

objects with small e but large q have a higher likelihood of having being scattered from the Oort cloud.

(2) Both 1I/'Oumuamua (2017 U1) and 2I/Borisov (2019 Q4) have orbits most consistent with an interstellar origin. While an origin by scattering from the Oort cloud cannot be rejected, this possibility has a very low probability of occurrence in the absence of a recent and very close stellar encounter, for which we have no evidence.

(3) We find that passing bodies of sub-stellar mass (down to ∼0.2 M_J) are capable of deflecting Oort cloud comets into hyperbolic orbits like those of 1I/'Oumuamua (2017 U1) and 2I/Borisov (2019 Q4).

Future observations of two kinds are needed to provide an improved understanding of the dynamics and origin of hyperbolic objects in the Solar system. First, the distribution of orbital elements of such bodies, especially in the eccentricity versus perihelion distance plane, will help determine the ratio of interstellar to scattered Oort cloud sources. Secondly, measurements of the abundance and distribution of sub-stellar (even sub-Jupiter) mass perturbers near the Sun are needed to quantify the role of scattering from the Oort cloud.

REFERENCES

Bannister M. T. et al., 2017, ApJ, 851, L38
Bolin B. T. et al., 2018, ApJ, 852, L2
Ćuk M., 2018, ApJ, 852, L15
de León J., Licandro J., Serra-Ricart M., Cabrera-Lavers A., Font Serra J., Scarpa R., de la Fuente Marcos C., de la Fuente Marcos R., 2019, Res. Notes Am. Astron. Soc., 3, 131
Dones L., Weissman P., Levison H. F., Duncan M., 2004, in Festou M. C., Keller H. U., Weaver H. A., eds, Comet II. Univ. Arizona Press, Tucson, AZ, p. 153
Engelhardt T., Jedicke R., Vereš P., Fitzsimmons A., Denneau L., Beshore E., Meinke B., 2017, AJ, 153, 133
Fitzsimmons A. et al., 2019, ApJL, 885, L9
Fraser W. C., Pravec P., Fitzsimmons A., Lacerda P., Bannister M. T., Snodgrass C., Igor, Smolić I., 2018, Nat. Astron., 2, 383
García-Sánchez J., Weissman P. R., Preston R. A., Jones D. L., Lestrade J. F., Latham D. W., Stefanik R. P., Paredes J. M., 2001, A&A, 379, 634
Jewitt D., Luu J., 2019, preprint (arXiv:1910.02547)
Jewitt D., Luu J., Rajagopal J., Kotulla R., Ridgway S., Liu W., Augusteijn T., 2017, ApJ, 850, L36
Knight M. M., Protopapa S., Kelley M. S. P., Farnham T. L., Bauer J. M., Bodewits D., Feaga L. M., Sunshine J. M., 2017, ApJ, 851, L31
Królikowska M., 2014, A&A, 567, A126
Królikowska M., Dybczyński P. A., 2017, MNRAS, 472, 4634
Królikowska M., Dybczyński P. A., 2019, MNRAS, 484, 3463
Luhman K. L., 2014, ApJ, 786, L18
Luhman K. L., Esplin T. L., 2016, AJ, 152, 78
Mashchenko S., 2019, MNRAS, 489, 3003
Meech K. J. et al., 2017, Nature, 552, 378
Micheli M. et al., 2018, Nature, 559, 223
Moro-Martín A., Turner E. L., Loeb A., 2009, ApJ, 704, 733
Mróz P. et al., 2017, Nature, 548, 183
'Oumuamua ISSI Team, 2019, Nat. Astron., 3, 594
Rafikov R. R., 2018, ApJ, 861, 35
Rickman H., Fouchard M., Froeschlé C., Valsecchi G. B., 2008, Celest. Mech. Dyn. Astron., 102, 111
Sumi T. et al., 2011, Nature, 473, 349
Williams G. V., 2017, MPEC 2017-U181: COMET C/2017 U1 (PANSTARRS). Available at: http://www.minorplanetcenter.net/mpec/K17/K17UI1.html
right E. L. et al., 2010, AJ, 140, 1868
Ye Q., Zhang Q., Kelley M. S. P., Brown P. G., 2017, ApJ, 851, L5

APPENDIX: DERIVATION

A1 Scattering angle

We assume a passing object that approaches the Sun on a hyperbolic orbit. Using non-rotational coordinates centred on the object having a given hyperbolic orbit defined by $V_{*\infty}$ and $b_\odot$, a comet encounters the object with the velocity and impact parameter V_* and b_{HOC}, respectively. The velocity of the object at the moment of the closest approach is given by

$$V_* = \sqrt{V_{*\infty}^2 + \frac{2GM}{r_*}}, \tag{A1}$$

where $M = m_\odot + m_*$. The angle between the velocity vectors of the comet before and after the encounter θ is given by

$$\tan\frac{\theta}{2} = \frac{Gm_*}{V_*^2 b_{HOC}}. \tag{A2}$$

Then, the velocity of the comet to the Sun after the encounter is expressed as

$$V = \sqrt{V_*^2 + V_*^2 - 2V_* V_* \cos\theta} = 2V_* \sqrt{\frac{\tan^2\frac{\theta}{2}}{1 + \tan^2\frac{\theta}{2}}}, \tag{A3}$$

For $\theta \ll 1$,

$$V = \frac{2Gm_*}{V_* b_{HOC}}, \tag{A4}$$

which is the velocity change given by the impulse approximation. Scattering that gives the velocity as large as the U1's, which is ∼V_*, cannot be dealt with using the impulse approximation. Equation (A3) gives

$$\tan\frac{\theta}{2} = \left(\frac{4V_*^2}{V^2} - 1\right)^{-\frac{1}{2}}. \tag{A5}$$

Next, we choose the non-rotating Cartesian coordinates centred on the Sun such that the x-axis is antiparallel to $\boldsymbol{V}_*$, the z-axis is antiparallel to the angular momentum vector of the object, and the y-axis is perpendicular to the x- and z-axes. The velocity vector of the comet after the encounter is expressed as $\boldsymbol{V} = V(\cos\alpha\cos\beta, \sin\alpha\cos\beta, -\sin\beta)$, where $\alpha = (\pi + \theta)/2$ is the angle between the x-axis and $\boldsymbol{V}$ and β is the angle between $\boldsymbol{b}_{HOC}$ and the reference plane. Using equation (A5), we have

$$\sin\alpha = \left(1 - \frac{V^2}{4V_*^2}\right)^{\frac{1}{2}}. \tag{A6}$$

A2 Object position

For the comet to have a trajectory with b after the encounter, the position of the object during the encounter must be determined. Let the angle between $\boldsymbol{r}_*$ and the x-axis be α_*. From the conservation

of angular momentum,

$$\sin \alpha_* = \frac{b_\odot V_{*\infty}}{r_* V_*}. \tag{A7}$$

By combining equations (A6) and (A7) and using equation (A1), we find r_* that gives V and b as

$$r_* = b_\odot \left(1 - \frac{V^2}{4V_{*\infty}^2}\right)^{-\frac{1}{2}} S, \tag{A8}$$

$$S = \left[1 + \left(\frac{GM}{V_{*\infty}^2 b_\odot}\right)^2 \left(1 - \frac{V^2}{4V_{*\infty}^2}\right)^{-1}\right]^{\frac{1}{2}}$$

$$\quad - \frac{GM}{V_{*\infty}^2 b_\odot}\left(1 - \frac{V^2}{4V_{*\infty}^2}\right)^{-\frac{1}{2}} \simeq 1, \tag{A9}$$

where $V_{*\infty} \neq 0$. The assumption of $S = 1$ corresponds to the approximation that the trajectory of the object is not hyperbolic but a straight line. We give $S = 1$ and $V_{*\infty} = V_*$ since this is true in almost all cases in this paper.

A3 Derivation of δg

The tiny volume δg is defined with the following equation so that comets contained within δg have V and b;

$$\delta g = \left|2\pi b_{\mathrm{HOC}} \delta b_{\mathrm{HOC}} \times V_* \times \frac{\delta \beta}{\pi}\right|, \tag{A10}$$

where the ring-area with the radius of b_{HOC} decides V and $\delta\beta$ gives the direction of V to meet the Sun with b. Using $b_\odot \gg b_{\mathrm{HOC}}$, the relation between β and b is

$$\beta \simeq \sin \beta = \frac{b}{r_* \sin \alpha}. \tag{A11}$$

Substituting equation (7) into equation (A11) and carrying out the differentiation, we obtain

$$\delta\beta = \frac{\delta b}{r_* \sin \alpha} = \frac{\delta b}{b_\odot}. \tag{A12}$$

The explicit expression of b_{HOC} is given from equations (A2) and (A5) as

$$b_{\mathrm{HOC}} = \frac{Gm_*}{V_*^2}\sqrt{\frac{4V_*^2}{V^2} - 1}. \tag{A13}$$

By carrying out the differentiation of equation (A13), we obtain

$$\delta b_{\mathrm{HOC}} = -4\frac{(Gm_*)^2}{V_*^2}V^{-3}b_{\mathrm{HOC}}^{-1}\delta V. \tag{A14}$$

Substituting equations (A12) and (A14) into equation (A10), we obtain δg as a function of V and b (equation 9).

A4 Coordinate transformation from impact parameters to orbital elements

From the relation of $V = \sqrt{Gm_\odot(e-1)/q}$ and $b = q\sqrt{(e+1)/(e-1)}$, the determinant of the Jacobian between the (V, b) and (e, q) frames is calculated as

$$J = \begin{vmatrix} \dfrac{\partial V}{\partial e} & \dfrac{\partial V}{\partial q} \\ \dfrac{\partial b}{\partial e} & \dfrac{\partial b}{\partial q} \end{vmatrix} = \frac{1}{2}\sqrt{\frac{Gm_\odot}{q(e+1)}}\frac{e}{e-1}. \tag{A15}$$

This paper has been typeset from a T$_{\mathrm{E}}$X/L$^{\mathrm{A}}$T$_{\mathrm{E}}$X file prepared by the author.